REPORT DOCUMENTATION PAGE

1. REPORT DATE (DD-MM-YYYY) 30-Sep-2008	2. REPORT TYPE REPRINT	3. DATES COVERED (From - To)

4. TITLE AND SUBTITLE	5a. CONTRACT NUMBER
FINITE-FREQUENCY SEISMIC TOMOGRAPHY OF BODY WAVES AND WAVES FROM AMBIENT SEISMIC NOISE: CRUSTAL AND MANTLE STRUCTURE BENEATH EASTERN EURASIA	FA8718-05-C-0017
	5b. GRANT NUMBER
	5c. PROGRAM ELEMENT NUMBER 62601F

6. AUTHOR(S)	5d. PROJECT NUMBER 1010
Yong Ren[2], Wei Zhang[1], Ting Yang[1], Yang Shen[2] ,and Xiaoping Yang[1]	5e. TASK NUMBER SM
	5f. WORK UNIT NUMBER A1

7. PERFORMING ORGANIZATION NAME(S) AND ADDRESS(ES)	8. PERFORMING ORGANIZATION REPORT NUMBER
Science Applications International Corporation 10260 Campus Point Drive San Diego, CA 92121-1152	

9. SPONSORING / MONITORING AGENCY NAME(S) AND ADDRESS(ES)	10. SPONSOR/MONITOR'S ACRONYM(S) AFRL/RVBYE
Air Force Research Laboratory 29 Randolph Road Hanscom AFB, MA 01731-3010	11. SPONSOR/MONITOR'S REPORT NUMBER(S) AFRL-RV-HA-TR-2008- 1078

12. DISTRIBUTION / AVAILABILITY STATEMENT

Approved for Public Release; Distribution Unlimited.

Science Applications International Corporation[1], University of Rhode Island[2], and Tongji University[1]

13. SUPPLEMENTARY NOTES

14. ABSTRACT

To improve seismic calibration for nuclear explosion monitoring, we use 3D sensitivity kernels of finite-frequency body and surface waves to develop models of the crustal and mantle structures beneath eastern Eurasia. We have collected and processed available broadband data from both permanent stations and temporary networks in eastern Eurasia. We obtained a regional P-wave velocity model for the mantle structures down to 1,500 km beneath the eastern Eurasia. We also carried out a detailed study of the P- and S-wave velocity structures in southeastern Tibet, which led to some interesting geological findings. Our P- and S-wave velocity models reveal a low-velocity anomaly in the crust and upper mantle to ~ 300 km depth beneath a north-south-trending rift zone in southeastern Tibet. This low-velocity anomaly is situated above a tabular, high-dipping-angle, high-velocity anomaly that extends into the upper-mantle transition zone. These results are evidence for the delamination of the mantle lithosphere and its causal relationship to the formation of the north-south trending rift in southeastern Tibet.

In order to improve models at shallow depths, we apply the finite-frequency methodology to the surface wave tomography using the ambient seismic noise. Unlike previous studies that calculated the dispersion curves from the estimated Green's functions to solve for phase or group velocity maps, we have developed a new approach using the 3D finite-frequency sensitivity kernels for the Green's functions. We have collected continuous data for stations in southeastern Tibet and computed the cross-correlations between all possible pairs of components from two stations. We constructed 3D sensitivity kernels for the estimated Green's functions derived from the cross-correlation of ambient noise, taking into account the effects of the surface topography. We will carry out a joint inversion of finite-frequency S-waves and estimated Green's functions, which are dominated by surface waves to resolve both the crustal and upper mantle structures.

15. SUBJECT TERMS

Seismic characterization, Finite Frequency Seismic Tomography, FFST

16. SECURITY CLASSIFICATION OF:			17. LIMITATION OF ABSTRACT	18. NUMBER OF PAGES	19a. NAME OF RESPONSIBLE PERSON Robert J. Raistrick
a. REPORT UNCLAS	b. ABSTRACT UNCLAS	c. THIS PAGE UNCLAS	SAR	10	19b. TELEPHONE NUMBER (include area code) 781-377-3726

DTIC COPY

FINITE-FREQUENCY SEISMIC TOMOGRAPHY OF BODY WAVES AND SURFACE WAVES FROM AMBIENT SEISMIC NOISE: CRUSTAL AND MANTLE STRUCTURE BENEATH EASTERN EURASIA

Yong Ren[2], Wei Zhang[2], Ting Yang[3], Yang Shen[2],and Xiaoping Yang[1]

Science Applications International Corporation[1], University of Rhode Island[2], and Tongji University[3]

ABSTRACT

To improve seismic calibration for nuclear explosion monitoring, we use 3D sensitivity kernels of finite-frequency body and surface waves to develop models of the crustal and mantle structures beneath eastern Eurasia. We have collected and processed available broadband data from both permanent stations and temporary networks in eastern Eurasia. We obtained a regional P-wave velocity model for the mantle structures down to 1,500 km beneath the eastern Eurasia. We also carried out a detailed study of the P- and S-wave velocity structures in southeastern Tibet, which led to some interesting geological findings. Our P- and S-wave velocity models reveal a low-velocity anomaly in the crust and upper mantle to ~ 300 km depth beneath a north-south-trending rift zone in southeastern Tibet. This low-velocity anomaly is situated above a tabular, high-dipping-angle, high-velocity anomaly that extends into the upper-mantle transition zone. These results are evidence for the delamination of the mantle lithosphere and its causal relationship to the formation of the north-south trending rift in southeastern Tibet.

In order to improve models at shallow depths, we apply the finite-frequency methodology to the surface wave tomography using the ambient seismic noise. Unlike previous studies that calculated the dispersion curves from the estimated Green's functions to solve for phase or group velocity maps, we have developed a new approach using the 3D finite-frequency sensitivity kernels for the Green's functions. We have collected continuous data for stations in southeastern Tibet and computed the cross-correlations between all possible pairs of components from two stations. We constructed 3D sensitivity kernels for the estimated Green's functions derived from the cross-correlation of ambient noise, taking into account the effects of the surface topography. We will carry out a joint inversion of finite-frequency S-waves and estimated Green's functions, which are dominated by surface waves to resolve both the crustal and upper mantle structures.

20081014127

OBJECTIVES

The main objective of this research is to construct high-resolution P-and S-velocity models of the crust and mantle beneath eastern Eurasia using 3D finite-frequency sensitivity kernels for body and surface waves. For surface wave tomography, we will utilize Green's functions derived from the cross-correlation of ambient noise at pairs of stations. A joint inversion of finite-frequency S waves and estimated Green's functions will be carried out to obtain the crust and mantle structure. The results will be used to improve seismic calibration for nuclear explosion monitoring.

RESEARCH ACCOMPLISHED

Finite-Frequency Seismic Tomography of Body and Surface Waves

1) Body Waves

To date, most global and regional tomographic studies are based on ray theory, where seismic waves are assumed to have an infinite frequency and the arrival time of a body wave phase depends only upon the wave speed along the geometrical ray path from the source to the receiver. However, because of wave front healing, scattering, and other diffraction effects, the travel time of a finite-frequency seismic wave is sensitive to a three-dimensional structure off the ray path. Based on the Born single-scattering approximation in conjunction with body wave ray theory, Dahlen et al. (2000) derived the formulation of the Born-Fréchet kernels for a seismic phase, which expresses the influence of velocity perturbations upon a finite frequency travel-time shift:

$$\delta t(\omega) = \int \int \int_{\oplus} K_b(\omega, \mathbf{x}) \frac{\delta c}{c}(\mathbf{x}) d^3\mathbf{x} \tag{1}$$

where the quantity $K_b(\omega,\mathbf{x})$ is the Fréchet sensitivity kernel over the 3D Earth structure for a travel-time shift δt measured by cross-correlation of an observed pulse with its synthetic one.

2) Surface Waves

Similarly, a measured surface-wave phase delay $\delta\Phi$ is written as a linear volumetric integration over heterogeneities of shear-wave and compressional-wave speed perturbations ($\delta\beta/\beta$ and $\delta\alpha/\alpha$) in the three-dimensional Earth (Zhou et al., 2006):

$$\delta\Phi(\omega) = \int \int \int_{\oplus} K_\beta(\omega, \mathbf{x}) \frac{\delta\beta}{\beta}(\mathbf{x}) d^3\mathbf{x} \quad \text{, for Love waves, and} \tag{2}$$

$$\delta\Phi(\omega) = \int \int \int_{\oplus} \left[K_\beta(\omega, \mathbf{x}) \frac{\delta\beta}{\beta}(\mathbf{x}) + K_\alpha(\omega, \mathbf{x}) \frac{\delta\alpha}{\alpha}(\mathbf{x}) \right] d^3\mathbf{x} \text{ , for Rayleigh waves,} \tag{3}$$

where ω is the angular frequency of surface waves, and K_β and K_α represent the phase sensitivity kernels related to the perturbations in the shear and compressional wave speeds, respectively.

In both cases of body and surface waves, according to equations 1, 2, and 3, the general problem for the inversion, after parameterization of the model function on a spatial grid of nodes, can be expressed as follows:

$$d_i = A_{il} m_l \tag{4}$$

where d_i is the ith measured body-wave travel-time shifts and surface-wave phase delays, A_{il} is the value of the integrated volumetric body-wave and surface-wave kernels, Kd^3x, contributing to the lth node, and m_l is the model parameter at the lth node.

High-Resolution P and S Velocity Models in Southeastern Tibet

We processed data from the Namche Barwa seismic experiment (Sol et al., 2007), which deployed a 50-station broadband array and a 20-element short-period array in southeastern Tibet during 2003–2004 (Figure 1). Data from the global seismographic network (GSN) station LSA, which is located close to this temporary network, are also included in this study. We used about 695 events that occurred during the operation period of the stations in 2003 and 2004, and with a magnitude greater than 5.5. With the multi-channel waveform cross-correlation method (VanDecar and Crosson, 1990), we measured differential travel times of teleseismic P and S waves between different stations for short, intermediate, and long periods: 0.5–2.0 Hz, 0.1–0.5 Hz, and 0.03–0.1 Hz for P waves, and, 0.1–0.5 Hz, 0.05–0.1 Hz, and 0.02–0.05 Hz for S waves. The P-differential travel times are measured on vertical component seismograms and those of S on traverse components. To avoid the ambiguity of long-period phase arrivals in the triplication range and the effects of the core-mantle boundary, we have considered only data with an epicentral distance of between 34° and 81°. Our final data set consists of ~ 36,313 P and ~15,043 S differential travel times, which are then utilized to invert for spatial variations in P- and S-wave velocity perturbations according to the 3-D finite-frequency kernel formulation (Dahlen et al., 2000; Hung et al., 2004; Yang et al., 2006).

Our results show the presence of a low-velocity anomaly in the crust and upper mantle down to a ~ 300-km depth beneath a north-south trending rift zone in southeastern Tibet (Figure 2) (Tapponnier and Molnar, 1977; Armijo et al., 1986; Yin, 2000). This low-velocity anomaly is situated above a tabular, high-dipping-angle, high-velocity anomaly that extends into the upper mantle transition zone. The Vp/Vs ratio of the high-velocity anomaly suggests that temperature variations are not the only cause and that a highly melt-depleted mantle is required. These results provide evidence for the mantle lithosphere delamination (Figure 3) and its link to north-south trending rifts in southeastern Tibet (Ren and Shen, 2008), contrary to previous studies that argued that the north-south trending rift zones in the Tibetan plateau are shallow features, formed by the eastward motion of the shallow crust decoupled from the mantle lithosphere by a low-viscosity lower-crust (e.g., Shen et al., 2001; Jiménez-Munt and Patt, 2006). Studies of an extended region in southern Tibet are thus needed to understand whether the mantle lithosphere delamination phenomenon is limited to the study area or occurs in a broad region where it plays an important role in the elevation and deformation of the Tibetan plateau.

Surface-Wave Tomography using Ambient Seismic Noise

Previous studies showed that the Rayleigh and Love Green's functions can be derived from the cross-correlation of ambient seismic noise on the three components (vertical, north and east) at pairs of stations, and that the ambient seismic noise tomography is an efficient method to image the crustal and shallow mantle structures with an improved path coverage and spatial resolution (Shapiro and Campillo, 2004; Sabra et al., 2005; Shapiro et al., 2005; Yao et al., 2006; Yang et al., 2007; Cho et al., 2007; Lin et al., 2008). In this project, we have applied the ambient seismic noise tomography to the region of southeastern Tibet to image the crustal and shallow upper mantle structures. But unlike previous studies that calculated the dispersion curves from the estimated Green's functions using an automated frequency-time analysis (FTAN) (Yao et al., 2006; Bensen et al., 2007; Yang et al., 2007; Cho et al., 2007) in order to solve for phase or group velocity maps, we are developing a new approach using the 3D finite-frequency sensitivity kernels for the Green's functions.

1) Data collection from Ambient Noise Cross-Correlation

We have collected and processed continuous data from about 70 stations deployed in the Namche Barwa seismic experiment during 2003–2004 (Figure 1, Sol et al., 2007). We have used all three components data (vertical, north, and east), and computed the cross-correlations between all possible pairs of components from two stations in order to obtain the estimated Green's functions. The raw data have been cut into 1-day-length waveforms, and the mean trend and instrument response are removed. All data are then bandpass filtered between periods of 4 s and 150 s, processed using the one-bit normalization, and stacked afterwards. Figure 4 shows an example of the cross-correlations (vertical-vertical, north-north, and east-east) between the Lhasa station LSA and the station ES11, bandpass filtered between 10s and 20s. The observed signals at both positive and negative correlation lag times

correspond to waves propagating in opposite directions between the stations. The Z-Z cross-correlation exhibits clearly the Rayleigh wave, whereas the N-N and E-E cross-correlations contain a combination of both Rayleigh and Love waves. The fact that surface wave waveforms are observed earlier on N-N and E-E cross-correlations than those on the Z-Z cross-correlation indicate effectively the presence of Love waves on the transversal components. The radial and transverse components, and thus first-order separation of Rayleigh and Love waves, can be obtained from the rotation of all possible combinations of cross-correlation of the three components (Lin et al., 2008). Figure 5 shows another example of the cross-correlations between the station LSA and all other stations for Z-Z, N-N, and E-E components, bandpass filtered between 10s and 20 s.

2) Sensitivity Kernels for Green's Function from Ambient Noise Cross-Correlation

In order to apply the finite-frequency methodology to the surface wave tomography using the ambient seismic noise, we have constructed 3D sensitivity kernels for the Green's function derived from the cross-correlation of ambient noise at pairs of stations. The kernels are calculated using the scattering integral method (Zhao et al., 2005; Zhang et al., 2007; Zhang and Shen, 2007). Because the Green's function derived from the cross-correlation of seismic ambient noise is the surface wave between pairs of stations, both the shallow velocity structure and surface topography may significantly affect the 3D sensitivity kernels. To assess the effects of surface topography on the sensitivity kernels, we put a band of random topography between the pair of stations. The topography is statistically characterized by a horizontal correlation length (a) and a height RMS (root mean square) fluctuation (ε) and has a Gaussian type autocorrelation function:

$$R(r) = \varepsilon^2 \exp^{-r^2/a^2}. \qquad (5)$$

Figure 6 shows an example of the 3D phase delay sensitivity kernels for a Green's function corresponding to the estimate from the cross-correlation of vertical records at two stations separated by 100 km in a modified ak135 model, in which the topography has a correlation length a=4 km and a height RMS fluctuation of 1 km. Our study shows that surface topography effect is most significant when the wavelength and the horizontal scale of surface topography are comparable (Zhang and Shen, 2007). This will occur if short-period waves are used. Thus in places with rough surface topography, the topographic effects must be taken into account in the use of short-period ambient noise.

Other Work

As shown in the previous report, we have obtained a regional P-wave velocity model for the upper 1,500 km beneath eastern Eurasia using the finite-frequency tomography methodology (Yang et al., 2006). We are collecting and processing additional data from the China National Seismic Network, which became available recently. The additional data will substantially improve the P-wave velocity model in this part of region. We will calculate travel-time corrections from the final P and S velocity models and relocate GT events with and without the corrections for model validation.

CONCLUSIONS AND RECOMMENDATIONS

We have applied the finite-frequency sensitivity kernels of body and surface waves to develop the crustal and mantle structures beneath eastern Eurasia. For the body-wave tomography, we have assembled a large data set of broadband waveforms and used cross-correlation to measure P and S differential travel times. The data set is then inverted for spatial variations in P- and S-wave velocity perturbations according to the 3D finite-frequency kernel formulation. P and S-wave velocity models beneath southeastern Tibet provide evidence for a causal relationship between the mantle lithosphere delamination and the north-south trending rifts. For the surface wave tomography using ambient seismic noise, we have collected continuous data from southeastern Tibet, and have computed the cross-correlations between all possible pairs of components in order to obtain the estimated Green's functions. In parallel, we have calculated the 3D sensitivity kernels for Green's functions derived from the cross-correlation of ambient noise at pairs of stations and have estimated the effects of surface topography on the sensitivity kernels. Both P- and S-wave velocity models derived from the finite-frequency tomography of body and surface waves will be used to improve seismic calibration in Eurasia.

REFERENCES

Armijo, R., P. Tapponnier, J. P. Mercier, and T. Han (1986). Quaternary extension in southern Tibet, *J. Geophys. Res.* 91: 13,803–13,872.

Bensen G. D., M. H. Ritzwoller, M. P. Barmin, A. L. Levshin, F. Lin, M. P. Moschetti, N. M. Shapiro, and Y. Yang (2007). Processing seismic ambient noise data to obtain reliable broad-band surface wave dispersion measurements, *Geophys. J. Int.* 169: 1239–1260, *doi: 10.1111/j.1365-246X.2007.03374.x.*

Cho, K. H., R. B. Herrmann, C. J. Ammon, and K. Lee (2007). Imaging the upper crust of the Korea Peninsula by surface-wave tomography, *Bull. Seism. Soc. Am.* 97 (1B): 198–207, doi: 10.1785/0120060096.

Dahlen, F. A., Hung, S.-H., and Nolet, G. (2000). Fréchet kernels for finite frequency traveltimes-I. Theory, *Geophys. J. Int.* 141: 157–174.

Hung, S.-H., Dahlen, F. A., and Nolet, G. (2000). Fréchet kernels for finite frequency traveltimes-II. Examples, *Geophys. J. Int.* 141: 175–203.

Hung, S-H ,Y. Shen, and L.-Y. Chiao (2004). Imaging seismic velocity structure beneath the Iceland hot spot: A finite frequency approach, *J. Geophy. Res.* 109: doi: 10.1029/2003JB002889.

Jimenez-Munt, I. and J.P. Platt (2006). Influence of mantle dynamics on the topographic evolution of the Tibetan plateau: Results from numerical modeling, *Tectonics* 25: TC6002, *doi:10.1029/2006TC001963.*

Lin F.-C., M. P. Moschetti, and M. H. Ritzwoller (2008). Surface wave tomography of the western United States from ambient seismic noise: Rayleigh and Love wave phase velocity maps, *Geophys. J. Int.* 173: 281–298, *doi: 10.1111/j.1365-246X.2008.03720.x.*

Ren, Y. and Y. Shen (2008). Tomographic evidence for a possible link between lithosphere delamination and the north-south trending rifts in Tibet, *J. Geophy. Res.*, under revision.

Sabra, K. G., P. Gerstoft, P. Roux, and W. A. Kuperman (2005). Extracting time-domain Green's function estimates from ambient seismic noise, *Geophys. Res. Lett.* 32: L03310, doi: 10.1029/2004GL021862.

Shapiro, N. M. and M. Campillo (2004). Emergence of broadband Rayleigh waves from correlations of the ambient seismic noise, *Geophys. Res. Lett.* 31: L07614, doi: 10.1029/2004GLL019491.

Shapiro, N. M., M. Campillo, L. Stehly, and M. H. Ritzwoller (2005). High-resolution surface-wave tomography from ambient seismic noise, *Science* 207: 1615–1618.

Shen, F., L. Royden, and B. C. Burchfiel (2001). Large-scale crustal deformation of the Tibetan plateau, *J. Geophys. Res.* 106 (B4): 6793–6816.

Sol, S., A. Meltzer, R. Burgmann, R. D. van der Hilst, R. King, Z. Chen, P. O. Koons, E. Lev, Y. P. Liu, P. K. Zeitler, X. Zhang, J. Zhang, and B. Zurek (2007). Geodynamics of the southeastern Tibetan Plateau from seismic anisotropy and geodesy, *Geology* 35: 563– 566, *doi:10.1130/G23408A.1.*

Tapponnier, P. and P. Molnar (1977). Active faulting and tectonics of China, *J. Geophys. Res.* 82: 2905– 2930.

VanDecar, J. C., and R. S. Crosson (1990). Determination of teleseismic relative phase arrival times using multi-channel cross-correlation and least squares, *Bull. Seismol. Soc. Am.* 80: 150–169.

Yang, T., Y. Shen, S. van der Lee, S. C. Solomon, and S. H. Hung (2006). Upper mantle structure beneath the Azores hotspot from finite-frequency seismic tomography, *Earth Planet. Sci. Lett.* 250: 11–26.

Yang, Y., M. H. Ritzwoller, A.L. Levshi, and N.M. Shapiro (2007). Ambient noise Rayleigh wave tomography across Europe, *Geophys. J. Int.* 168: 259–274.

Yao, H., R. D. van der Hilst, and M. V. de Hoop (2006). Surface-wave array tomography in SE Tibet from ambient seismic noise and two-station analysis –I. Phase velocity maps, *Geophys. J. Int.* 166: 732–744, *doi: 10.1111/j.1365-246X.2006.03028.x.*

Yin, A. (2000). Mode of Cenozoic east-west extension in Tibet suggesting a common origin of rifts in Asia during the Indo-Asian collision, *J. Geophys. Res.* 105: 21,745–21,759.

Zhang, Z., Y. Shen, and L. Zhao (2007). Finite-frequency sensitivity kernels for head waves, *Geophys. J. Int.* 171: 847–856, *doi:10.1111/j.1365-246X.2007.03575.x.*

Zhang, W. and Y. Shen (2007). Finite-frequency tomography using ambient seismic noise in the presence of surface topography, *AGU Fall Meeting Abstracts*, B1384.

Zhao, L., T. H. Jordan, K. B. Olsen, and P. Chen (2005). Frechet kernels for imaging regional earth structure based on three-dimensional reference models, *Bull. Seism. Soc. Am.* 95: 2066–2080.

Zhao, L. and T. H. Jordan (2006). Structural sensitivities of finite-frequency seismic waves: a full-wave approach, *Geophys. J. Int.* 165: 981–990, *doi:10.1111/j.1365-246X.2006.02993.x.*

Zhou, Y., F. A. Dahlen, and G. Nolet (2005). Three-dimensional sensitivity kernels for surface wave observables, *Geophys. J. Int.* 158, 142–168, *doi:10.1111/j.1365-246X.2004.02324.x.*

Zhou, Y., F. A. Dahlen, G. Nolet, and G. Laske (2005). Finite-frequency effects in global surface-wave tomography, *Geophys. J. Int.* 153: 1087–1111, *doi:10.1111/j.1365-264X.2005.02780.x.*

Zhou, Y., G. Nolet, F. A. Dahlen, and G. Laske (2006). Global upper-mantle structure from finite-frequency surface-wave tomography, *J. Geophys. Res.* 111: B04304, *doi:10.1029/2005JB003677.*
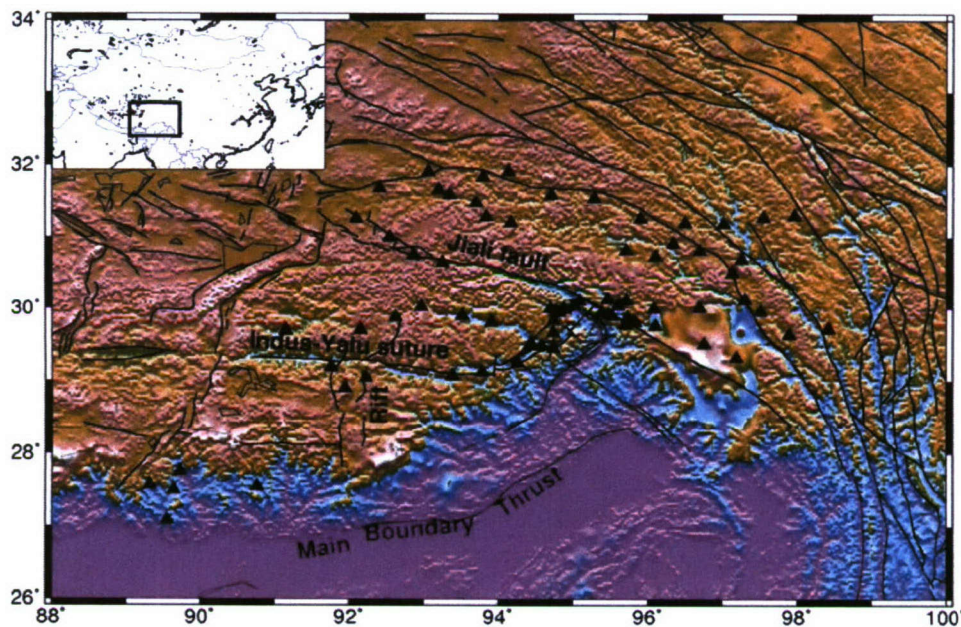
Figure 1. Topographic map of southeastern Tibet with active faults in the region of the Himalayan Eastern syntaxis and the locations of the stations used in the study.
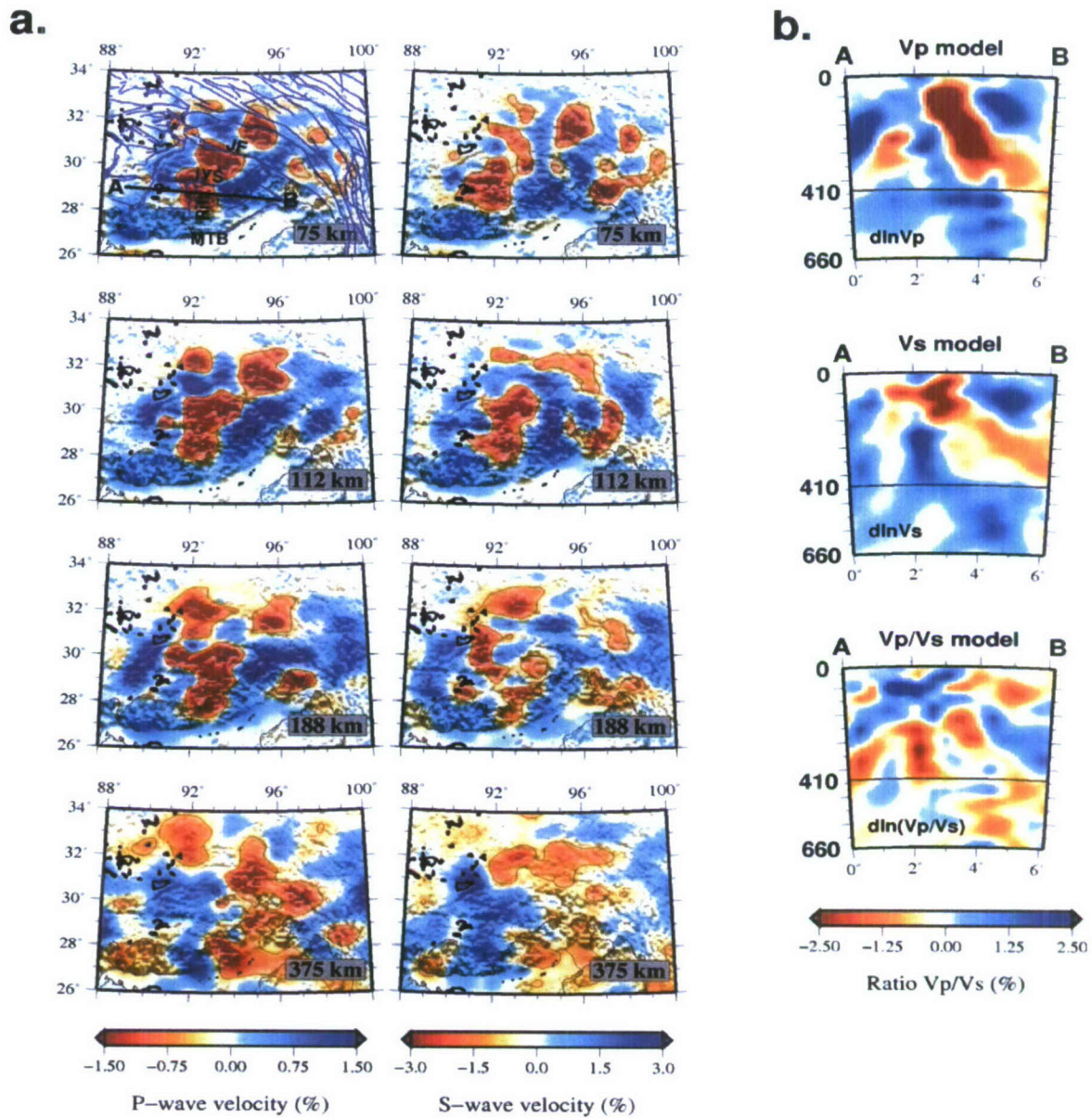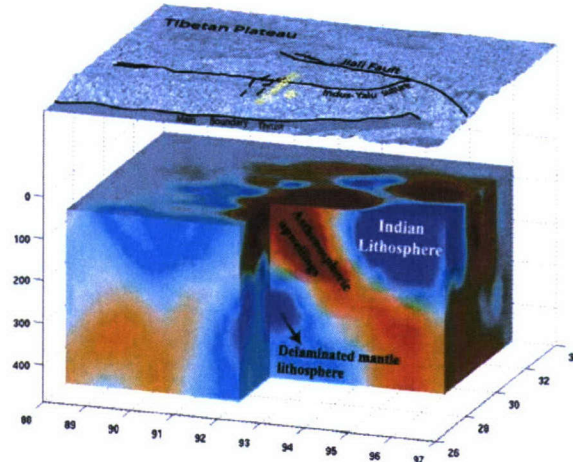
Figure 2. (a). P- and S-wave velocity perturbations relative to the reference model (CRUST2.0 and iasp91) at different depths: 75 km, 112 km, 188 km and 375 km. (b). Cross-section A-B through P- and S-wave tomographic models, along the Indus-Yarlung suture and across the rift in southeastern Tibet. Topographic map of southeastern Tibet with active faults in the region of the Himalayan Eastern syntaxis and the locations of the stations used in the study.

Figure 3. Three-dimensional image of the P-wave velocity model with our interpretation of the observed structures in southeastern Tibet. The topography is not to scale.
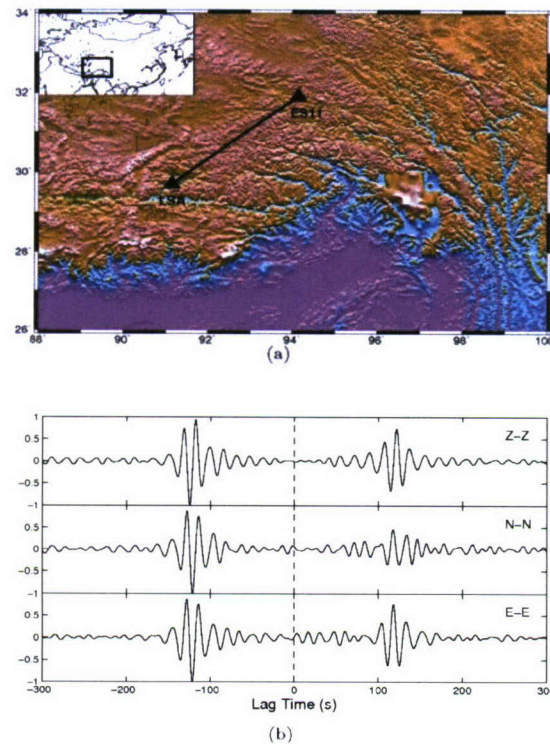

Figure 4. (a). The path between the GSN station LSA (Lhasa, Tibet) and the station ES11. (b). The 10–20 s bandpass filtered cross-correlations observed between the station LSA and ES11, as showed in a). The labels Z-Z, N-N and E-E denote the cross-correlation between Vertical-Vertical, North-North and East-East components, respectively.
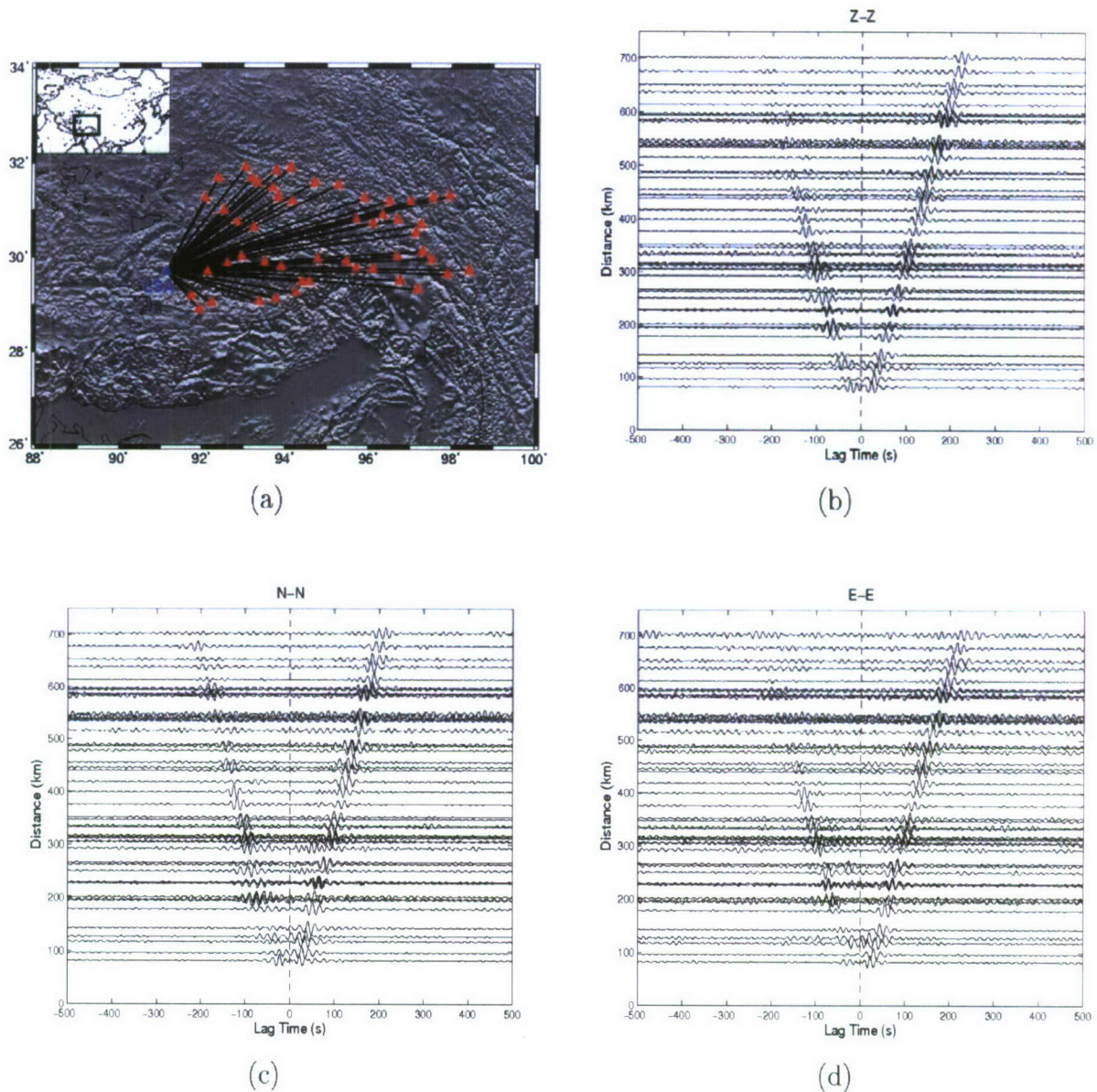
(a)

(b)

(c)

(d)

Figure 5. (a). The path between the GSN station LSA (Lhasa, Tibet) and the stations deployed in the Namche Barwa seimic experipment. (b–d). The bandpass filtered (10–20 s) cross-correlations observed between the station LSA and other stations for Z-Z (Vertical-Vertical), N-N (North-North), and E-E (East-East) components.
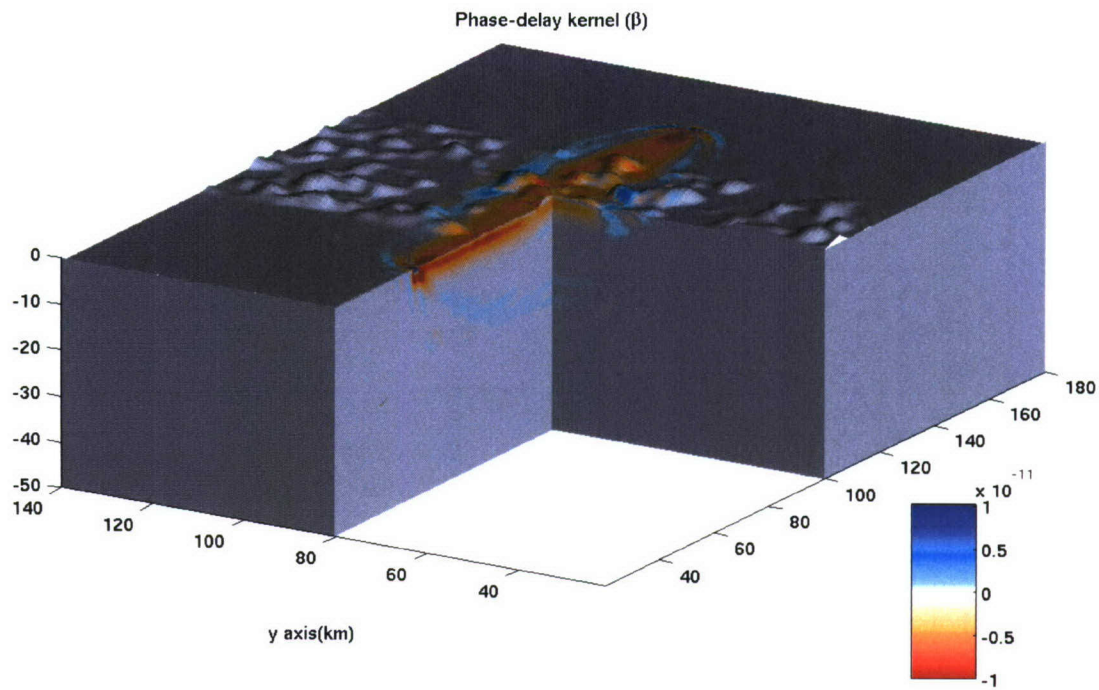
Figure 6. Sensitivity kernels for a modified model ak135 with the topography having a correlation length a=4 km, RMS=1 km, and the center frequency of the source time function fc=0.5 Hz. The center wavelength is around 6 km, and the horizontal length of a single hill is around 8-9 km. The horizontal scale of the hill is greater than one wavelength. The topography-scattered waves cause some sensitivities at depth, and the kernels are distorted by the topography.